

Optical tweezers system measuring the change in light momentum flux

Wilfried Grange, Sudhir Husale, Hans-Joachim Güntherodt, and Martin Hegner^{a)}

Institute of Physics, National Center of Competence in Research (NCCR) Nanoscale Science, University of Basel, Klingelbergstrasse 82, CH-4056 Basel, Switzerland

(Received 19 October 2001; accepted for publication 13 March 2002)

This article describes the design of a dual-beam optical tweezers (OT) instrument which, in contrast to conventional single-beam OT, directly measures the change in light momentum flux when a trapped object experiences a force. Consequently, no local calibration is needed to measure the force acting on a trapped particle. The instrument has a high trapping efficiency and forces up to 200 pN can be measured. In addition, the above-mentioned system operates in conjunction with a three-dimensional steerable single-beam OT. © 2002 American Institute of Physics.

[DOI: 10.1063/1.1477608]

I. INTRODUCTION

It was first demonstrated in 1970 by Ashkin that light could be used to trap and accelerate dielectric micron-sized particles.¹ For these experiments, a stable optical potential well was formed using two—slightly divergent—counterpropagating laser beams. This pioneer study established the groundwork for the well-known optical tweezers (OT) technique, where a single laser beam is focused by a high numerical aperture (NA) objective lens to a diffraction-limited spot.² At the focal point, not only dielectric spheres can be trapped, but also biological organisms such as cells, virus, or bacteria, as shown in 1987 by Ashkin and co-workers.^{3,4} The considerable interest of biologists for the OTs technique comes from the fact that minute forces can be also measured with sub-pN accuracy on the trapped object.⁵ Since such small forces are not accessible by conventional techniques such as scanning-force-microscopy-based techniques (in liquid and at room temperature), OT has become a major investigation tool in biology (see Refs. 6 and 7 for recent reviews).

In the ray-optics regime, known as the Mie regime, the origin of optical forces can be understood easily. Since a bundle of light rays is refracted when passing through a dielectric object, existing rays have a different direction than incoming rays. This results in a change in the light momentum. By conservation of momentum, the change in the light momentum causes a change in the momentum of the trapped particle. As a result, the particle will feel a force. Optical forces are, however, very small, since ~ 100 mW of power at the focus produces only forces of tens of pN. It can be shown that stable trapping occurs along the optical axis when the *gradient force* (which is, to a good approximation, proportional to the spatial gradient of the light) overcomes the *scattering force* (caused by Fresnel reflections at the surface and directly proportional to the intensity of the light). This explains why (i) high-NA objective lenses have to be used and (ii) the back aperture of the objective lens has to be over-

filled. In principle, the change in the direction of the refracted rays can be observed on a detector. In this case, a collecting lens, such as a condenser lens, is placed after the objective lens and converts angular deflections into transverse deviations $X(Y)$. An important point is that the deviations $X(Y)$ are directly proportional to the change in light momentum flux (the force), if and only if all rays are collected⁸ (the proportionality constant depends on the known instrument parameters, see Sec. II A). For a single-beam OT, this latter condition is never fulfilled because of the light scattering at the back aperture of the objective lens that introduces marginal rays. Therefore, an OT instrument has to be calibrated by some means. One of the most accurate calibration procedures consists in determining (i) the light lever stiffness (in pN nm^{-1}) from the thermal power spectrum and (ii) the detector sensitivity (in V nm^{-1} , to relate nanometer displacements of the particle in the trap with volts). Since both the trap stiffness and the detector sensitivity depend on local parameters (laser power, size or index of refraction of the particle, local fluid viscosity, etc.), they have to be determined for each new experiment. This is certainly an important drawback of the OT technique. To overcome these limitations, one has to collect all the rays and, therefore, to underfill the back aperture of the objective lens. In this case, the spatial gradient of the light will be too small to overcome the scattering force and trapping cannot be stable. An appealing route to have a stable trapping without overfilling the back aperture of the objective lens is to use two counterpropagating laser beams that focus on the same point.⁹ As a result, scattering forces, which act only in the direction of the beam, will compensate each other and stable trapping is possible. To our knowledge, Smith and co-workers first describe in 1996 the use of a dual-beam OT instrument to investigate the mechanical properties of single molecules.¹⁰ This work studied the response of a ds-DNA single molecule stretched beyond its entropically regime and revealed, thanks to the high trapping efficiency of dual-beam OTs, the existence of an overstretching plateau at 68 pN. Latter, dual-beam OTs have lead to fascinating progress in single-molecule studies. For instance, dual-beam OTs have been used to investigate (i) the folding–unfolding transitions

^{a)}Electronic mail: Martin.Hegner@unibas.ch

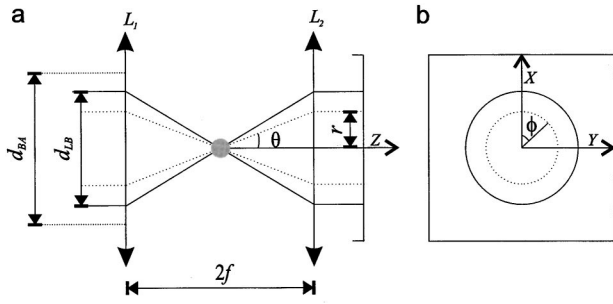


FIG. 1. Schematic representation of the lens system and definition of angular coordinates. (a) A laser beam (full diameter d_{LB}) enters an objective lens L_1 (back aperture diameter d_{BA}). The focused rays are collected by a condenser lens, identical to the objective lens. We assume $d_{LB} \leq d_{BA}$ so that no scattered rays are present. A ray (dotted line), exiting a particle (gray sphere) at an angle θ with respect to the optical axis (Z direction), hits the detector at a radial height $r = nf \sin \theta$. (b) Scheme of the detector. Also are introduced the angle ϕ and the unit vectors \hat{i} and \hat{j} (X and Y directions, respectively). Note that the two lasers should focus at different locations along the Z direction (see Ref. 9).

of single Titin molecules,¹¹ (ii) the polymerization of individual RecA-DNA filaments,¹² (iii) the activity of polymerase enzymes,¹³ (iv) the unfolding of single RNA molecules,¹⁴ and (v) the package of DNA in viruses.¹⁵

Although dual-beam OTs have been used over the past six years, a detailed description about the possible implementation of such instruments has not been yet given. In this article, we describe a dual-beam OT instrument, based on the principles mentioned above, and which does not suffer from the limitations of conventional single-beam OTs. In particular, it will be shown that this new instrument acts as a force transducer by measuring directly (i.e., without any local calibrations needed) the change in light momentum flux. The trapping efficiency of this instrument is larger than single-beam OTs, which is of prime importance for biological investigations. In addition, a third trap (fully steerable in three dimensions) is implemented and allows us to handle micron-sized objects with ~ 40 nm accuracy in the specimen plane (Sec. III).

II. DUAL-BEAM OPTICAL TWEEZERS

A. Theoretical considerations

We consider the following experimental setup (shown in Fig. 1), where a laser beam is focused by an objective lens L_1 and is collected with a condenser lens L_2 .¹⁶ We furthermore assume that (i) the diameter of the laser beam is much smaller than the back aperture of the objective lens, (ii) L_1 and L_2 are identical and corrected for infinity (i.e., a collimated laser beam is focused at the focal length of the lens), and (iii) L_1 and L_2 form an afocal system (i.e., a collimated laser beam emerges as a collimated beam). In the following, f will denote the focal length of the two lenses, d_{BA} the diameter of the back aperture, and d_{LB} the full diameter of the laser beam. For simplicity, we will now assume that the diameter of the particle d is larger than the wavelength λ so that a ray optics picture is sufficient to calculate the trapping force (i.e., we vector sum the momentum of all light rays).

The force F exerted by the laser light onto a particle is simply the difference in light momentum flux between the rays entering the particle and the rays exiting the particle. For a bundle of rays, the momentum flux is given by nW/c , where n is the index of refraction of the surrounding medium, W the power of the light (in watts), and c the speed of light. Using angular coordinates, F can be written as⁸

$$F = \frac{n}{4\pi c} \oint I(\theta, \phi) (\hat{i} \sin \theta \cos \phi + \hat{j} \sin \theta \sin \phi + \hat{k} \cos \theta) d\gamma, \quad (1)$$

where θ and ϕ are defined in Fig. 1, $I(\theta, \phi)$ is the intensity in watts per steradian [$I(\theta, \phi)$ is negative for rays entering the particle], and $d\gamma$ is an element of the solid angle ($d\gamma = \sin \theta d\theta d\phi$). A detector placed after L_2 converts angular deviations into transverse deviations. Therefore, one can rewrite Eq. (1) as¹⁷

$$F^* = \frac{1}{cf} \oint E(r, \phi) (r[\hat{i} \cos \phi + \hat{j} \sin \phi]) dA. \quad (2)$$

In the above equation, F^* denotes the transverse force felt by the particle, r is the radial height of a ray exiting the particle with an angle θ ($r = nf \sin \theta$), $E(r, \phi)$ is the intensity per unit area on the detector (in W m^{-2}), and dA is an element of area on the detector ($dA = r dr d\phi$). It is natural to decompose Eq. (2) into two components F_X and F_Y for the X (along the \hat{i} axis) and Y (along the \hat{j} axis) directions, respectively,

$$F_X = \frac{1}{cf} \oint E(r, \phi) (\hat{i} r \cos \phi) dA, \quad (3a)$$

$$F_Y = \frac{1}{cf} \oint E(r, \phi) (\hat{j} r \sin \phi) dA. \quad (3b)$$

The right-hand sides of Eqs. (3a) and (3b) are quantities that can be measured with a position sensing detector (PSD). Indeed, a two-dimensional PSD allows a separation of the X and Y components and can be designed to give output currents I_X and I_Y that are related to the weighted component of the light intensity as follows:

$$I_X = \alpha \int E(X, Y) \frac{X}{R} dX dY, \quad (4a)$$

$$I_Y = \alpha \int E(X, Y) \frac{Y}{R} dX dY, \quad (4b)$$

where $2R$ is the effective length of the PSD (i.e., the distance between the two electrodes), and α is a factor describing the efficiency of the detector (V W^{-1} at the trap). Identifying Eqs. (3) and (4) gives the simple result:

$$F_X = \frac{I_X R}{c \alpha f}, \quad (5a)$$

$$F_Y = \frac{I_Y R}{c \alpha f}. \quad (5b)$$

In conclusion, the force acting on a particle can be determined without any local calibration since the quantities R , α , and f depend only on instrument parameters that do not vary

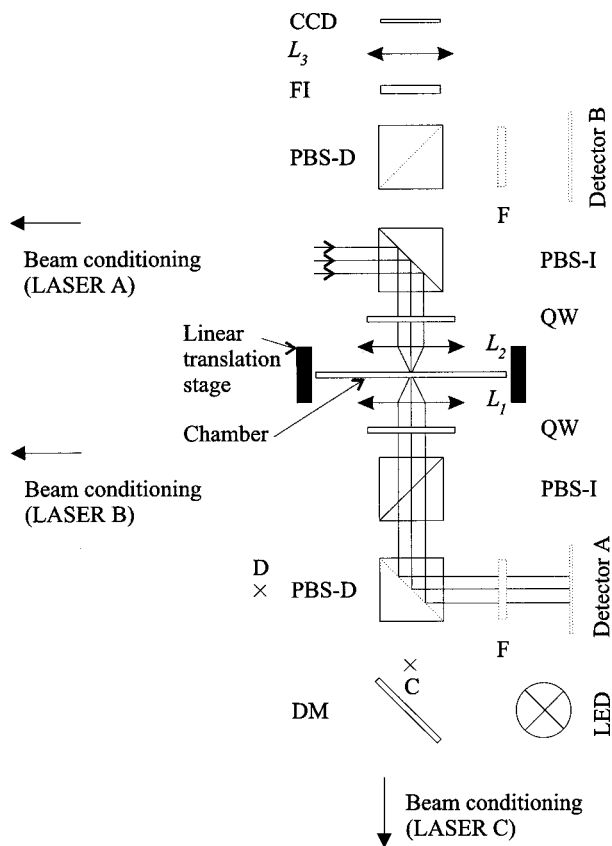


FIG. 2. Experimental setup required for the injection and detection of the two counterpropagating laser beams. Dotted lines show elements that are not in the plane of the optical table. L_1 (L_2), injection and detection lens; PBS, polarized beam splitter; QW, quarter-wave plate; and F, low-pass filter. Note that L_2 is placed onto a piezoelectric element (gray rectangle). Also shown is the imaging part: LED, light-emitting diode (480 nm); DM, dichroic mirror; and FI, low-pass filters for imaging. L_3 is a planoconvex lens used to image the focal plane of L_2 on a CCD camera. The chamber is placed on an independent piezoelectric element (gray rectangle). See Secs. II B 1 and II B 4 for explanations.

with the experimental conditions. It is obvious that Eqs. (5a) and (5b) hold only in the case where all light rays are collected. Therefore, a dual-beam instrument is needed (Sec. I). Let us finally mention that Eqs. (5a) and (5b) have been derived using ray optics theory. In the following sections, we will see, however, that the instrument we have built still works properly when the latter approximation is *a priori* not fulfilled.

B. Instrument design

1. Injection and detection of the lasers

Since two counterpropagating laser beams are used to trap a single particle, it is important to be able to detect transverse deviations for one laser (say, *A*) without any perturbation (e.g., loss of power) on the other laser (say, *B*). This problem is solved by the use of polarized beam splitters (PBS) (03PBS064, Melles Griot, Irvine, CA) and quarter-wave (QW) plates (QWPO-830-08-4-R10, CVI, Albuquerque, NM), as described in detail below.

Figure 2 shows the experimental setup used to (i) inject the two lasers and (ii) detect transverse deviations (i.e., forces). As described previously (Sec. II A), this experimen-

tal setup consists of two identical water immersion lenses [UPLAPO 60X/W/IR, Olympus, Zürich, Switzerland (NA = 1.2, $d_{BA} = 7.2$ mm, 285 μm working distance)] that form an afocal optical system.^{18,19} Before entering a lens, the collimated laser, which has been conditioned to have a (1, -1, 0, 0) polarization state (vertical *p* state in Stokes notations)²⁰ is reflected by a PBS element (PBS-I). When passing through the two lenses and the two QWs, the state of light polarization is first changed to (1, 0, 0, 1) and then to (1, 1, 0, 0) (horizontal *p* state). Therefore, the next PBS (PBS-I) transmits the laser beam. Finally, a third PBS (PBS-D) redirects the laser beam to a two-dimensional PSD detector (detector A) (DL-10, UDT, Hawthorne, CA). Since this setup is fully symmetric, laser *B* [incoming polarization state (1, -1, 0, 0)] can be also injected and detected without any significant loss of power on detector *B*. For laser *A*, parasite reflections measured at points *C* and *D* are smaller than 2% (see Fig. 2). Similar values have been obtained for laser *B*.

As shown in Sec. I, the two counterpropagating lasers *A* and *B* have to be superimposed (i.e., they should nearly focus at the same point) to allow a high trapping efficiency. For this reason, lens L_2 is placed onto a XYZ flexure stage (MDT631, Thorlabs, Newton, NJ) operated by a three-axis piezocontroller (MDT690, Thorlabs, Newton, NJ).

2. Beam shaping and conditioning

Since we underfill the back aperture of microscope lenses L_1 and L_2 , trapping along the *Z* axis with a single laser beam is far from being stable. However, we need—for alignment procedures—to be able to trap with a single beam, at least when small forces (< 20 pN) are applied. For this reason, beam shaping and conditioning have to be done carefully and have to minimize as possible optical aberrations and wave-front distortions (see Fig. 3 for a schematic representation of the experimental setup).

Each single-mode diode laser [5431-G1, SDL, San Jose, CA ($\lambda = 830$ nm, maximum power 200 mW)] is driven with an external module (laser diode driver model 505, Newport, Irvine, CA) and is temperature controlled (temperature controller model 325, Newport, Irvine, CA).²¹ The collimated delivered beam is Gaussian TEM₀₀ mode and rectangular shaped ($\sim 5.2 \times 1.7$ mm). The diode laser has been mounted to deliver a (1, 0, 1, 0) polarized beam. Beam shaping is achieved using anamorphic prisms (06GPA004, Melles Griot, Irvine, CA) that produce a square-shaped beam (~ 5.2 mm, full length). To prevent back reflections and reduce mode hopping of the laser, we use optical isolators (IO-5-830-LP, Optics for Research, Caldwell, NJ). Note that the electric field experiences a 45° rotation when passing through this latter optical element. Therefore, the state of polarization is now (1, -1, 0, 0). Finally, the beam is spatially filtered using two identical achromat doublets (focal length: 100 mm) and a 40 μm pinhole [mounted on an XYZ lens positioner (LP-1-XYZ, Newport, Irvine, CA)]. After this filtering, the laser beam shows a clean Gaussian profile with an isotropic circular shape ($d_{LB} \sim 5$ mm) and can be finally injected through the microscope lenses.

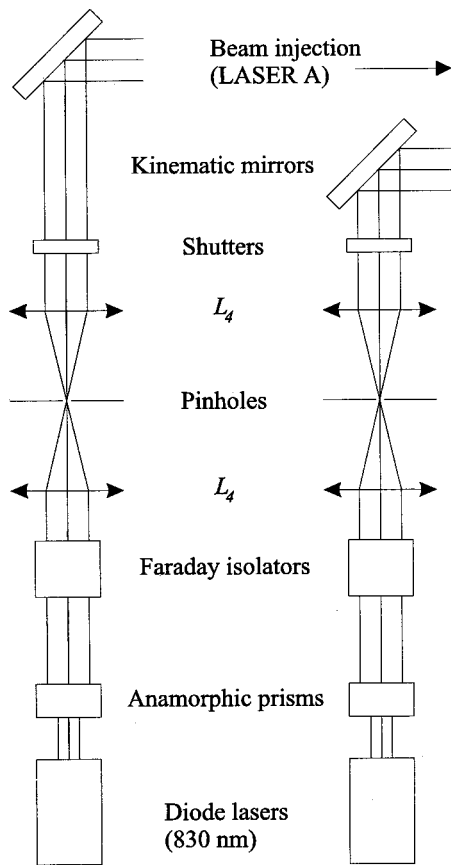


FIG. 3. Double-beam conditioning. A description of parts can be found in the text (Sec. II B 2). Note (i) that the separation between the two lenses L_4 (focal length f_4) is chosen as $2f_4$ and (ii) kinematic mirrors are used to redirect the beam onto the PBS (Fig. 2).

The above-described arrangement has been found to allow for precise conditioning and to minimize loss of power through the different optical element. For a maximum output power of 200 mW of the laser diode, we measure a value of ~ 75 mW at the trap focus.

3. Detector

For each laser, a two-dimensional PSD detector directly measures the quantities I_X and I_Y (in volts) that appear in Eqs. (4a) and (4b) and that are relevant to determine the force [Eqs. (5a) and (5b)]. In addition, a voltage, directly proportional to the light intensity, is readout from each PSD. To reduce noise, the electronic circuit (needed for proper signal conditioning) is placed in a shielded box next to the detector.

4. Chamber, imaging, flow system

The chamber and flow system we use is similar to the ones described in Ref. 22. Typically, the chamber itself consists of two parafilm layers sealed on two microscope coverglass No. 1. Prior to sealing, the parafilm layers are cut to define a channel ($50 \times 3.5 \times 0.3$ mm) for fluid injection and a ~ 100 μm glass tube (inner diameter) is inserted between the parafilm layers. Two holes are drilled within the chamber to define an inlet and an outlet for liquid. The ~ 300 - μm -thick chamber is then placed on an aluminum holder. A glass mi-

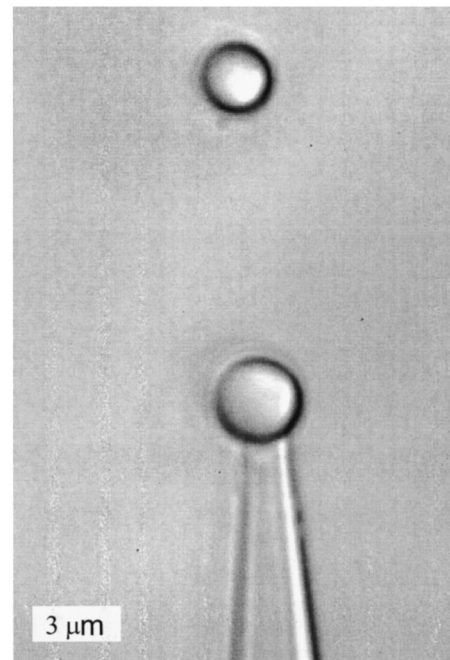


FIG. 4. Typical image of the micropipette (aperture < 1 μm) holding a polystyrene bead (diameter, 3.10 μm). The polystyrene bead in the upper part of the image (diameter, 2.90 μm) is trapped by the two counterpropagating laser beams. For a typical stretching experiment, a single molecule is placed between the two beads and the micropipette (placed onto a piezoelectric element) is moved with nanometer accuracy.

cropipette is pulled from a glass capillary (outer diameter ~ 80 μm) to obtain a < 1 μm diam on one side. The micropipette is finally inserted inside the ~ 100 μm tube and connected to a manual syringe to allow suction of micron-sized beads. An important point is that the nearly coincident focus of the two counterpropagating laser beams defines a fixed location in space (Sec. II B 1). For this reason, the chamber has to be placed on an element that allows movements in three-dimensions, independently of the XYZ flexure stage used to align the lasers. This element is composed of two one-dimensional translation stages (TSX-1D, Newport, Irvine, CA) that have a 25 mm travel range in the Z direction. These stages hold a three-axis piezoelectric flexure scanner (517.3CL, Physik Instrumente, Waldbronn, Germany) that has a maximum extension of 100 μm for the X and Y directions and 20 μm along the Z axis, respectively (Fig. 2). Each axis is operated by a voltage signal (0–100 V) provided by an amplifier module (E-503.00, Physik Instrumente, Waldbronn, Germany). This voltage is controlled by an analog signal (0–10 V) applied to the standard coaxial inputs of the amplifier. For accurate movements (closed-loop operation), a servocontroller (E-509.C3, Physik Instrumente, Waldbronn, Germany) is also used.

For a typical experiment, the pipette and the trapped bead have to be imaged onto a charge-coupled-device (CCD) camera (Fig. 4). A planoconvex lens L_3 is, therefore, used to image the specimen plane (the focus of the objective lenses) onto the chipset of the CCD camera (VCB-3424, MSM Trading, Basel, Switzerland). Light is provided by a light-emitting diode (LED) ($\lambda = 480$ nm), which is first reflected by a dichroic mirror (600DRLP, Omega Optical, Brattleboro,

VT) and then injected into L_1 (Fig. 1). The pipette is brought to the specimen plane using both manual translation stages and a piezoelectric device (see above). Note, finally, that additional low-pass filters [labeled FI in Fig. 2 (Schott, Feldbach, Switzerland)] are used to eliminate unwanted IR radiation on the CCD.

Fluid delivery is controlled using pressure bottles and an automatic valve system (MVP, Hamilton, Reno, NV). Pressure bottles are used either to contract or expand the air on the different buffer solutions, which are afterwards injected in the chamber by the valve system.²² The flow rate in the chamber is directly proportional to the difference in height between the liquid in the buffer solution and the waste solution (connected to the outlet of the chamber) times the applied pressure (vacuum). In contrast to peristaltic pumps, such a system has no mechanical parts and, therefore, produces steady flow streams with pN accuracy.

5. Automation

We use Labview (National Instruments, Austin, TX) to fully control and operate our instrument. Two cards [PCI-6031E and PCI-6704, 16 bits resolution, 100 kSamples/s (National Instruments, Austin, TX)] allow us (i) to output voltages on the different piezoelectric elements, (ii) to acquire analog signals from the detectors and the pressure sensors, and (iii) to control the shutters (846HP, Newport, Irvine, CA). In addition, the valve system is controlled via the serial port of the PC through a PXI-1002 chassis (National Instruments, Austin, TX). Finally, we use a frame grabber (PCI-1408, National Instruments, Austin, TX) to process images acquired on the CCD camera.

C. Results

We already have emphasized that the main advantage of the dual-beam OT lies in the fact that we measure directly the difference in light momentum flux (Secs. I and II A). Therefore, we are able to determine the force acting on the trapped particle without any knowledge of the trap stiffness. In other words, the instrument should always give a correct measure of the force acting on the particle even if some local parameters (e.g., power of the laser, index of refraction, etc.) change. In this section, we first briefly describe the calibration procedure needed to determine the force from output detector signals. As a benchmark test, we pull a dsDNA single molecule beyond its entropically regime. Then, we demonstrate that the calibration is independent of local variables (laser power, size of the trapped particle). Finally, the performances of the instrument are highlighted.

1. Calibration procedure and overstretching of dsDNA

The calibration only needs to be done once since only the quantities α [the detector efficiency, V W^{-1} (at the trap)] and R (the effective radius of the detector, m) have to be known to get the force [Eqs. (5a) and (5b)]. Other quantities (i.e., focal length) are obtained from the manufactures. α can be easily determined using a power meter, and R using a collimated laser mounted on an XY translation stage.

To test this calibration, we have recorded the force as a function of the displacement of a trapped particle (in the

TABLE I. Stiffness of the optical trap ($\text{pN } \mu\text{m}^{-1}$) determined from (i) force vs displacement measurements (K^*) and (ii) the corner frequency of the power spectral density of the force fluctuations (Sec. II C 1) (K^\bullet). Stiffnesses have been measured for different bead sizes and different laser powers at the focus. Also shown is the percentage of light collected by the microscope lenses.

Diameter (μm)	K^* ($\text{pN } \mu\text{m}^{-1}$)		K^\bullet ($\text{pN } \mu\text{m}^{-1}$)		Light collected (%)
	150 mW	80 mW	150 mW	80 mW	
7.00	57 ± 5	29 ± 3	61 ± 3	31 ± 3	>99
3.10	144 ± 9	73 ± 6	144 ± 4	74 ± 3	>99
1.87	265 ± 12	140 ± 10	256 ± 5	138 ± 4	>99
0.60	140 ± 10	72 ± 6	154 ± 5	80 ± 5	97

specimen plane), while gradually increasing the speed of the flow in the chamber. From the slope of the force versus displacement plots,²³ the value of the trap stiffness K can be determined (Table I). Alternatively, the stiffness of an optical trap (i.e., for a low Reynolds number) can be estimated from the power spectral density $S_{\text{FF}}(f)$ of the thermal force fluctuations using⁵

$$S_{\text{FF}}(f) = \frac{2kT\gamma f^2}{\pi(f^2 + f_c^2)}, \quad (6)$$

where γ is the viscous drag, f_c the corner frequency [$f_c = (2\pi\gamma)^{-1} \text{K}$], and $kT = 4.1 \text{ pN nm}$ at room temperature. For our experiment, spherical particles are used and are trapped far away from the chamber walls. Therefore, the viscous drag is easily computable. As a consequence, the trap stiffness can be determined, independently of the calibration procedure.⁵

As seen in Table I, the stiffness values measured using (i) a robust and widely used calibration method (thermal fluctuations) and (ii) the change in light momentum flux are in good agreement. This comes from the fact that nearly all the rays are collected with our high-NA condenser lens, even when diffraction effects are expected to be important (i.e., $\lambda \leq d$). This last result undoubtedly demonstrates the validity of the calibration procedure.

As a typical benchmark test, we show in Fig. 5 a typical overstretching curve of a single 10 kbp ds-DNA molecule. For this experiment, a micron-sized polystyrene bead (Bangs laboratories, Fishers, IN)—coated with Streptavidin receptors—was first trapped by the lasers. The micropipette was approached close enough to the bead and suction was applied with a syringe to hold this $3.10\text{-}\mu\text{m}$ -diam bead on the clear aperture of the micropipette (Fig. 4). The micropipette was then retracted away from the trap and a second bead (coated with one ds-DNA, $2.90 \mu\text{m}$ in diameter) was injected in the chamber and trapped. The activation of this latter bead follows the procedure described in Ref. 24. Briefly, it consists of (i) chemically activating the microsphere and covalently attaching a thiol-modified 5'-end of the dsDNA to the surface of the bead and (ii) attaching a Biotin ligand group to the other 3'-end. Since Biotin and Streptavidin have a strong affinity, the experiment consists of moving the micropipette around the trapped bead until a hookup is felt on the detectors.

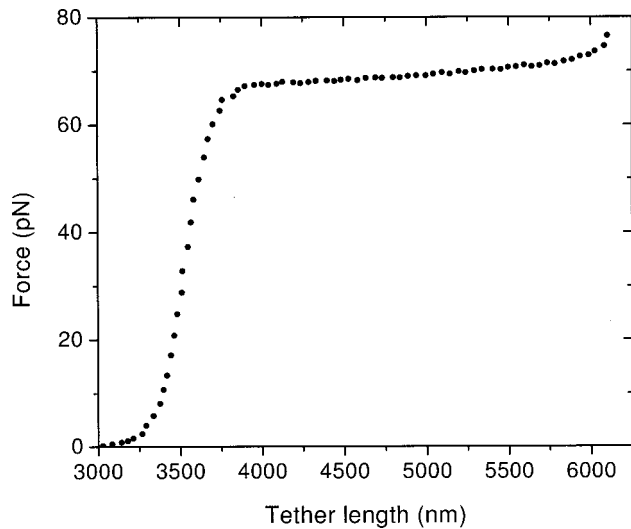


FIG. 5. Typical overstretching curve obtained on a single 10 kbp ds-DNA molecule [150 mM NaCl, Hepes buffer pH 7.5]. Note that the length of the dsDNA was inferred from the distance of the two beads (see Ref. 23).

The DNA overstretching curve (Fig. 5) shows, as expected, a plateau at 68 pN (*S* transition) [150 mM NaCl, Hepes buffer pH 7.5], in excellent agreement with previous experiments.^{10,12,25}

2. Power and bead size dependence

Figure 6 shows the force acting on a polystyrene microsphere (3.10 μm in diameter) as a function of the speed of flow. For a total power of 150 mW, the force shows—as expected—a linear behavior as a function of the applied pressure. Decreasing the total power of the laser should not affect the force acting on the trapped particle but should dramatically decrease the trapping efficiency. In other words, the stiffness of the light lever is modified when the power of the lasers is changed (see the inset of Fig. 6) and a new calibration should be performed for a single-beam OT instrument to accurately determine the force acting on the trapped particle. With our instrument we, however, directly measure the change in light momentum flux. Therefore, the force versus applied pressure plots measured for different laser powers show a unique linear dependence.

We now demonstrate that the momentum flux sensor is independent of the bead size. For this purpose, different bead sizes were trapped by the lasers and the detector outputs were recorded as a function of the fluid velocity [Fig. 7(A)]. According to Stokes law, the slopes S_{Stokes} of the obtained curves should be proportional to the diameter of the trapped particles. As a result, the quantity $F/v_{\text{flow}} = S_{\text{Stokes}}$ (i.e., the frictional force divided the fluid velocity) should be a linear function of the bead diameter. This is exactly what is obtained in our measurements [Fig. 7(B)].

3. Thermal noise and trapping efficiency

The thermal noise level (pN²/Hz) of the instrument has been obtained from the power spectrum measured with a 16 bit card over a large bandwidth (10–50 kHz).⁵ For a 3.10-μm-diam bead, the noise level is constant (white noise) for frequencies below 785 Hz (corner frequency f_c) and about

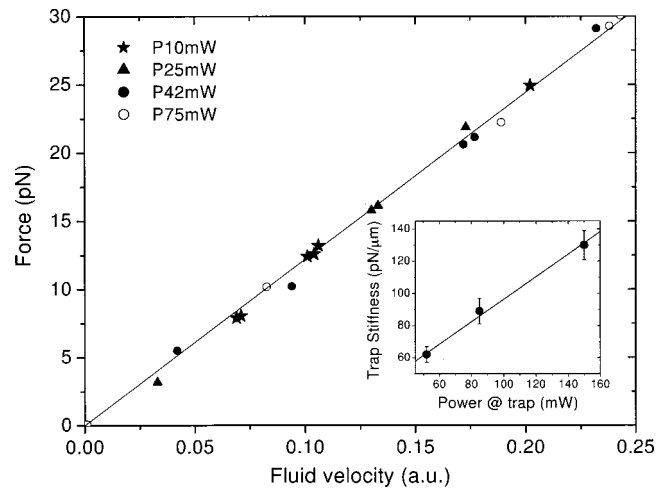


FIG. 6. Force as a function of the fluid velocity (3.10-μm-diam bead). Empty circles, 150 mW; filled circles, 84 mW; triangles, 50 mW; stars, 20 mW. Solid line, linear fit to the data. In the inset is shown the dependence of the trap stiffness as a function of the total laser power (i.e., for the two laser beams). Note that the trap stiffness can be easily obtained from a fit of the power spectrum with a Lorentzian function (Sec. II C 1).

$4 \gamma k T = 4.7 \times 10^{-4} \text{ pN}^2/\text{Hz}$ [Eq. (6)]. This noise is mainly of thermal origin since other sources of noise have been minimized. The noise drops rapidly for frequencies above f_c and reaches a value of about $1 \times 10^{-7} \text{ pN}^2/\text{Hz}$ for frequencies above 40 kHz. As mentioned above (Sec. II C 1), this behavior is characteristic of a particle that has a low Reynolds number and that moves in a parabolic potential well.⁵ Note, finally, that for a typical experiment the detector signal is low-pass filtered to cut high frequencies and to prevent aliasing.

The performance of the instrument can be discussed in terms of a dimensionless factor Q , known as the trapping efficiency. Q is related to the maximum trapping force F_{trap} and the laser power P through the following relation:

$$F_{\text{trap}} = nQP/c. \tag{7}$$

The Stokes law calibration (Sec. II C 2) allows us to determine F_{trap} . We found values of 200, 145, and 36 pN, for bead diameters of 3.10, 1.87, and 0.60 μm, respectively. This gives Q values of 0.30, 0.22, and 0.05, respectively. Clearly,

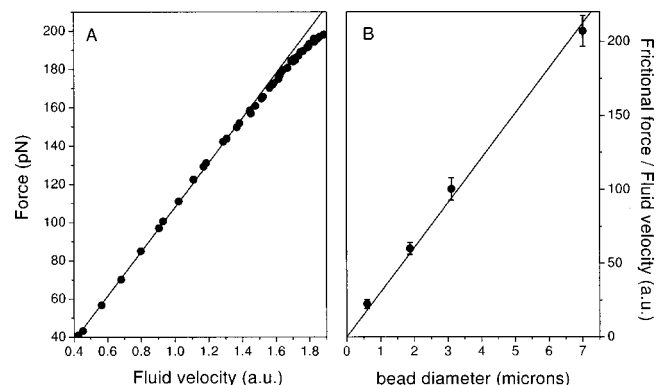


FIG. 7. (A) Force as a function of the applied pressure (3.10-μm-diam bead). Note that the force readings start to be nonlinear at ~170 pN (Sec. II D). (B) Ratio of the frictional force and the fluid velocity as a function of the bead diameter. Solid lines, linear fits to the data.

the momentum flux sensor shows a high trapping efficiency and reaches high forces as compared to single-beam OTs. For instance, the maximum force that can be applied on a micron-size bead with single-beam OTs is only of about 60 pN.^{19,26}

D. Discussion

In the previous sections, we have shown that the calibration procedure is independent of both the power of the lasers and the size of the particle. But, we also have checked that the calibration of the instrument is independent of other local parameters such as the index of refraction of the particle or the surrounding buffer, and the shape of the trapped particle (not shown).⁸

An important assumption made for the derivation of Eqs. (5a) and (5b) is that all the rays are collected. If this would not be the case, then the detector readings would be inaccurate. For all bead sizes investigated (0.60, 1.87, 3.10, and 7.00 μm), the percentage of light collected by the condenser lens was larger than 97. This, therefore, indicates the validity of the approach we have used. We emphasize that the use of low-NA lenses (smaller than 1), possible with dual-beam OTs,⁸ is not recommended when using bead sizes comparable to the wavelength of the laser. Indeed, scattering effects are important in this case. As a consequence, the percentage of light collected after the condenser lens will be probably smaller than 90%, which reduces the accuracy of the instrument. Moreover, the force readings can be inaccurate for a high-NA lens when the force is so high that part of the laser spot hits the back aperture of the lens. For our lens ($d_{\text{BA}} = 7.2 \text{ mm}$, $f = 3 \text{ mm}$), and the size of the laser ($d_{\text{LB}} \sim 5 \text{ mm}$), the force readings start to be inaccurate for forces greater than $\sim 170 \text{ pN}$ at full laser power [Fig. 7(A)], well above any reported force involved in biological transitions or molecular motor processes.^{6,7}

Let us finally point out that dual-beam OTs, if much more powerful than single-beam OTs, suffer also from limitations. Among them, optical drift is a real nuisance in the experiment and has to be corrected [e.g., by the use of a piezoelectric element placed on one of the microscope objectives (Sec. II B 1)]. This procedure has been automatized in our instrument.

III. THIRD TRAP

As seen the previous sections, lasers *A* and *B* share a common focus, which defines a fixed location in space for the trap. As a consequence, the trapped bead cannot be steered (with the above-described setup) in three-dimensions. We now describe the implementation of a single-beam OT (used as a handle) that allows movements of another trapped object with a $\sim 40 \text{ nm}$ accuracy in the specimen plane. In the following sections, we will use the same notations as in Sec. II.

A. Requirements for a steerable trap

Because a single-beam OT is used to steer the trap, the back aperture of the microscope has to be overfilled (Sec. I). Moreover, the incoming laser beam (laser *C*) should pivot

around the objective entrance aperture to ensure a stable trapping when moving the trap. In their review paper, Svoboda and Block⁵ have presented many experimental setups that fulfill this latter requirement. Among them, the use of a piezoelectric gimbal mirror, which is placed in a plane conjugate to the back aperture of the microscope, is certainly best suited (see below).²⁷ Indeed, such an arrangement allows fast steering of the trap²⁸ and has less constraints (in terms of distances between the different optical elements) than usual steering setups.

1. Steering in the specimen plane (*X*, *Y* directions)

To steer the beam in the specimen plane, we need to image the back aperture of the microscope lens (e.g., L_1 , Fig. 2) onto a device that has angular movements only (e.g., a gimbal mirror). To accomplish this, two lenses [say, L'_{xy} (focal length f'_{xy}) and L''_{xy} (focal length f''_{xy})] have to be inserted between the back aperture of the microscope lens and the gimbal mount. Moreover, the relationship between the distances d_{gs} [between the plane of rotation of the gimbal mount and L'_{xy} (the lens closest to the gimbal)] and d_{sb} (between L''_{xy} and the back aperture of the microscope) should be given by²⁷

$$d_{gs} = \frac{f'_{xy}}{f''_{xy}} \left[f'_{xy} + f''_{xy} - \frac{f'_{xy}}{f''_{xy}} d_{sb} \right], \quad (8)$$

where we have assumed—for simplicity—that L'_{xy} and L''_{xy} are forming an afocal system. Under this condition [Eq. (8)], a tilt of θ of the gimbal mirror will induce a displacement of $\sim 2ff'_{xy}\theta/f''_{xy}$ in the specimen plane (i.e., *X* and *Y* directions).

2. Steering along the *Z* direction

As outlined by Fällman and Axner,²⁷ the beam can also be steered along the *Z* direction if two additional steering lenses [say, L'_z (focal length f'_z) and L''_z (focal length f''_z)] are placed in front of the gimbal mirror. When (i) L''_z (the lens which is closest to the gimbal) is placed at a distance of f''_z away from the gimbal and (ii) the distance between L'_z and L''_z is about $f'_z + f''_z$, a movement of L'_z along the *Z* direction will change the divergence of the beam without changing the size of the beam on the gimbal mirror (i.e., the degree of overfilling of the microscope lens). In this case, a translation of L'_z along the *Z* direction induces a change δz_{trap} of the focus (the specimen plane) along the *Z* direction equal to²⁷

$$\delta z_{\text{trap}} = \left(\frac{ff'_{xy}}{f''_{xy}f''_z} \right)^2 \delta z. \quad (9)$$

Let us point out that the *Z* steering is of peculiar importance in our instrument since lasers *A* (*B*) and *C* do not have the same divergence.

B. Instrument design

For the third beam, we use a diode laser emitting at 1064 nm (LCS-DTL-322, Laser 2000, Wessling, Germany). The beam has a TEM₀₀ beam diameter of $\sim 1.5 (1/e^2)$ and is linear polarized (maximum output power: 1 W). The laser

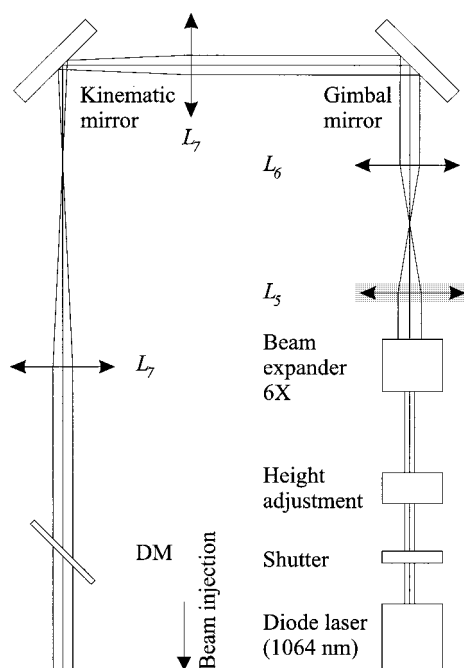


FIG. 8. Setup for the steerable third trap. Note that (i) the dichroic mirror (DM) is the same as the one shown in Fig. 2 and (ii) lens L_5 is placed on a translation stage (gray rectangle). The back aperture of the microscope lens L_1 (Fig. 2) is imaged onto the plane of rotation of the gimbal mirror with the use of two identical lenses L_7 that form—in our instrument—an afocal system.

beam is first brought at a correct height (similar to that of lasers A and B) using an X-beam steerer, composed of two 45° mirrors (Fig. 8). To achieve proper overfilling of the microscope back aperture (lens L_1), a $6\times$ beam expander (S6ASS0106, Sill Optics, Wendelstein, Germany) is then implemented within the path. For Z steering (Sec. III A 2), we use two lenses L_5 (focal length: 80 mm) and L_6 (focal length: 62.9 mm). These two lenses form an afocal arrangement and L_5 is placed onto a piezoelectric element (MDT631, Thorlabs, Newton, NJ), which is operated by a piezocontroller (MDT690, Thorlabs, Newton, NJ) and an additional dc-stepper motor. The XYZ flexure stage (used only in the Z direction) has a piezoelectric translation of $15\ \mu\text{m}$ and a manual translation of 2 mm. This results in a maximum change in depth of focus of $\sim 35\ \text{nm}$ and $\sim 4.6\ \mu\text{m}$ for the piezoelectric and dc operations, respectively [Eq. (9), see below for the specifications of the XY -steering lenses].

Beam steering along the X and Y directions (in the specimen plane) is achieved by pivoting a gimbal mount (U200-G, Newport, Irvine, CA). For precise movements of the gimbal, we use closed-loop dc actuators (CMA-12CCL, Newport, Irvine, CA) driven by a ESP300 platform (Newport, Irvine, CA). With such a configuration, the minimal incremental angular motion of the gimbal is 7×10^{-6} rad, yielding a minimal incremental motion of $\sim 42\ \text{nm}$ in the specimen plane (Sec. III A 1). The XY -steering lenses [labeled L_7 (focal length: 175 mm) in Fig. 8] also are placed in an afocal arrangement and follow the requirements (in terms of position) mentioned in the preceding section.

After proper conditioning of the laser, the laser beam passes through a dichroic mirror (see Figs. 2 and 8) and

enters microscope lens L_1 . At the entrance back aperture of L_1 , we measured a $1/e^2$ diameter of $\sim 7.1\ \text{mm}$. It is important to note that the PBS used to inject lasers A and B transmits most of the 1064 nm laser beam. However, parasitic back reflections of the 1064 nm laser beam can interfere with the output readings of the detectors A and B (Fig. 2). To prevent this, we use low-pass filters [labeled F in Fig. 2 (Schott, Feldbach, Switzerland)].

C. Discussion

The steering system presented in the previous sections is found to allow precise three-dimensional movements of the trap in the specimen plane with minimal loss of the light when pivoting the laser beam around the entrance back aperture of the microscope lens. Moreover, it allows micron-sized movements of the trap in all three dimensions. We checked, also (by measuring the escape force on detector A and B as a function of the flow speed), that this third trap has a reasonable trapping efficiency, comparable to that of single-beam OTs. The third trap will enable the local probing with sub-pN resolution of biological interactions along a filamentous molecule attached between the pipette and the dual-beam tweezers. Among these interactions are protein-DNA interactions¹³ and filamentous proteins (e.g., actin or tubulin) interacting with other proteins (the targeting molecule will then be attached to the third bead). This third possibility is of great relevance for localization of individual targets of the investigated systems which might differ on the specific location of the interacting biological systems.

ACKNOWLEDGMENTS

This work was supported by the Swiss National Science Foundation (Grant Nos. 31-61497.00 and 2160-056392.99), the Treubel Foundation, and the National Competence Center for Research (NCCR) “Nanoscale Science” network. The authors would like to acknowledge Steven B. Smith for fruitful discussions.

¹A. Ashkin, Phys. Rev. Lett. **24**, 156 (1970).

²A. Ashkin, J. M. Dziedzic, J. C. Bjorkholm, and S. Chu, Opt. Lett. **11**, 288 (1986).

³A. Ashkin and J. M. Dziedzic, Science **235**, 1517 (1987).

⁴A. Ashkin, J. M. Dziedzic, and T. Yamane, Nature (London) **330**, 769 (1987).

⁵K. Svoboda, and S. M. Block, Annu. Rev. Biophys. Biomol. Struct. **23**, 247 (1994).

⁶A. D. Mehta, M. Rief, J. A. Spudich, D. A. Smith, and R. M. Simmons, Science **283**, 1689 (1999).

⁷C. Bustamante, J. C. Macosko, and G. J. L. Wuite, Nat. Rev., Mol. Cell Biol. **1**, 130 (2000).

⁸S. B. Smith, Ph.D. thesis, University of Twente, The Netherlands (1998).

⁹Due to Fresnel reflections of incident light rays at the surface of the trapped particle, the focus of two lasers should be slightly different along the Z direction.

¹⁰S. B. Smith, Y. J. Cui, and C. Bustamante, Science **271**, 795 (1996).

¹¹M. S. Z. Keller Mayer, S. B. Smith, H. L. Granzier, and C. Bustamante, Science **276**, 1112 (1997).

¹²M. Hegner, S. B. Smith, and C. Bustamante, Proc. Natl. Acad. Sci. U.S.A. **96**, 10109 (1999).

¹³G. L. J. Wuite, S. B. Smith, M. Young, D. Keller, and C. Bustamante, Nature (London) **404**, 103 (2000).

¹⁴J. Liphardt, B. Onoa, S. B. Smith, I. Tinoco, Jr., and C. Bustamante, Science **292**, 733 (2001).

- ¹⁵D. E. Smith, S. J. Tans, S. B. Smith, S. Grimes, D. L. Anderson, and C. Bustamante, *Nature (London)* **413**, 748 (2001).
- ¹⁶The denomination used here (objective lens, condenser lens) is to some extent arbitrary since lenses L_1 and L_2 play the same role.
- ¹⁷This integral runs over the detector, which only measures the change in light momentum flux for exiting rays. Since the momentum flux for incident rays is independent of the force, it represents only a constant offset value in Eq. (1).
- ¹⁸Until recently, high-NA water immersion lenses were not commercially available. Therefore, oil immersion lenses had to be used. Although such lenses produce a steep spatial gradient, the difference in the index of refraction between oil and water (inside the chamber) dramatically increases spherical aberrations, when the focus is brought away from the chamber wall. As a result, a single beam trap which uses oil immersion lenses can only trap within a distance of $\sim 20 \mu\text{m}$ away from the chamber wall. Nowadays, high-NA (1.2) water immersion lenses overcome such limitations. For instance, they allow a stable trapping at distances greater than $\sim 150 \mu\text{m}$ away from the surface.
- ¹⁹L. P. Ghislain, N. A. Switz, and W. W. Webb, *Rev. Sci. Instrum.* **65**, 2762 (1994).
- ²⁰W. Bickel and W. Baile, *Am. J. Phys.* **53**, 468 (1985).
- ²¹The 830 nm wavelength is best suited for biological investigations due to the relative transparency of biological materials and water at this wavelength. K. C. Neuman, E. H. Chadd, G. F. Lion, K. Bergman, and S. M. Block, *Biophys. J.* **77**, 2856 (1999).
- ²²G. L. J. Wuite, R. J. Davenport, A. Rappaport, and C. Bustamante, *Biophys. J.* **79**, 1155 (2000).
- ²³For these measurements, video microscopy was used to track the location of the trapped bead in the specimen plane. The CCD camera was calibrated using a $10\text{-}\mu\text{m}$ -increments calibration grid (one pixel equals 48 nm). Using IMAQ libraries from Labview (National Instruments, Austin, TX) that have subpixel accuracy, movements as small as ~ 7 nm can be easily detected.
- ²⁴M. Hegner, *Single Mol.* **1**, 139 (2000).
- ²⁵M. Rief, H. Clausen-Schaumann, and H. E. Gaub, *Nat. Struct. Biol.* **6**, 346 (1999).
- ²⁶R. M. Simons, J. T. Finer, S. Chu, and J. A. Spudich, *Biophys. J.* **70**, 1813 (1996).
- ²⁷E. Fällman and O. Axner, *Appl. Opt.* **36**, 2107 (1997).
- ²⁸C. Mio, T. Gong, A. Terray, and D. W. M. Marr, *Rev. Sci. Instrum.* **71**, 2196 (2000).